Journal of Hazardous Materials 219–220 (2012) 156–163

Contents lists available at SciVerse ScienceDirect

Journal of Hazardous Materials

journal homepage: www.elsevier.com/locate/jhazmat

Iron phthalocyanine/TiO_2 nanofiber heterostructures with enhanced visible photocatalytic activity assisted with H_2O_2

Zengcai Guo[a], Bin Chen[a,*], Jingbo Mu[a], Mingyi Zhang[b], Peng Zhang[b], Zhenyi Zhang[b], Jingfeng Wang[a], Xin Zhang[b], Yangyang Sun[b], Changlu Shao[b,*], Yichun Liu[b]

[a] Department of Chemistry, Northeast Normal University, 5268 Renmin Street, Changchun 130024, People's Republic of China
[b] Center for Advanced Optoelectronic Functional Materials Research, Key Laboratory of UV Light-Emitting Materials and Technology of Ministry of Education, Northeast Normal University, 5268 Renmin Street, Changchun 130024, People's Republic of China

ARTICLE INFO

Article history:
Received 12 December 2011
Received in revised form 24 March 2012
Accepted 26 March 2012
Available online 3 April 2012

Keywords:
TiO_2
Phthalocyanine
H_2O_2
Nanofiber
Photocatalysis

ABSTRACT

One-dimensional 2,9,16,23-tetra-nitrophthalocyanine iron(II) (TNFePc)/TiO_2 nanofiber heterostructures have been successfully obtained by a simple combination of electrospinning technique and solvothermal process. The as-obtained products were characterized by field emission scanning electron microscopy (FE-SEM), energy-dispersive X-ray (EDX) spectroscopy, transmission electron microscopy (TEM), X-ray diffraction (XRD), X-ray photoelectron spectroscopy (XPS), and IR spectrum. The results revealed that the TNFePc nanosheets were successfully grown on the primary TiO_2 nanofibers. And, the coverage density of the secondary TNFePc nanostructures could be controlled by adjusting the experimental parameters. Photocatalytic tests displayed that the H_2O_2 assisted TNFePc/TiO_2 nanofiber heterostructures (TNFePc/TiO_2–H_2O_2) possessed a much higher degradation rate of methyl orange than the pure TiO_2 and TNFePc/TiO_2 nanofiber without H_2O_2 under visible light. Moreover, the TNFePc/TiO_2 nanofiber heterostructures could be easily recycled without the decrease of the photocatalytic activity due to their one-dimensional nanostructural property of TiO_2 nanofibers.

1. Introduction

Nowadays, organic pollutants constitute an important family of pollutants of wastewater produced by chemical, petrochemical, food-processing or textile industries. Due to the urgent need for a clean and comfortable environment, photocatalysis becomes a hot topic of research for the elimination of toxic chemicals in the environment through its efficiency and broad applicability [1,2]. As a cheap, non-toxic, green and highly efficient photocatalyst, titanium dioxide (TiO_2) has been extensively studied and applied to mineralize various organic contaminants transforming them into inorganic species or converting them into organic species readily biodegradable [3]. However, one severe disadvantage of this semiconductor material is the large band gap of 3.2 eV for anatase form, which limits its photoresponse to the ultraviolet (UV) region as it is excited at 387 nm. It greatly limits the use of sunlight as an energy source for the photoreaction since only about 3–4% of solar light falls in the UV range [4–6]. Therefore, its applications are still limited. To efficiently utilize solar energy, many attempts have been undertaken to make this process responsive to visible light, such as doping ions, compound, acid treatment, etc. [7–9]. Although the degradation efficiency is partly improved, the potential effects are unknown. For instance, doped materials suffer from thermal instability, photocorrosion, lattice distortion, and an increase in the carrier-recombination probability [10]. Other methods may result in secondary pollution in environment. Thus, we need one effective reagent, which can effectively modify the surface of TiO_2 and leave no pollution in the environment.

In our previous work, the metallophthalocyanines sensitized TiO_2 catalysts exhibited a good photocatalytic activity of common organic pollutants by the formation of the MPc/TiO_2 heteroarchitectures. The as-prepared MPc/TiO_2 heteroarchitectures could hinder the charge recombination and improve the photocatalytic efficiency. Meanwhile, phthalocyanines can be fixed onto TiO_2, which could avoid phthalocyanines enter into the environment to cause additional pollution [11]. However, this heteroarchitectures catalyst is not effective enough for the degradation of azo dyes, which are widely dispersed in industrial wastewater and long persistence as environmental hazards in water. Therefore, there is a need to enhance reaction rate of photocatalysis for efficient and rapid treatment of these pollutants during practical wastewater treatment. According to previous researches [12], H_2O_2 assisted photocatalysis have been shown to be potentially advantageous

* Corresponding authors. Tel.: +86 43185098803.
E-mail addresses: chenb608@nenu.edu.cn (B. Chen), clshao@nenu.edu.cn (C. Shao).

0304-3894/$ – see front matter © 2012 Elsevier B.V. All rights reserved.
http://dx.doi.org/10.1016/j.jhazmat.2012.03.068

and useful in the treatment of the compounds that are difficult to degradation. Highly reactive and non-selective hydroxyl radicals that have the ability to oxidize most of the azo dyes in industrial effluents are produced by H_2O_2 assisted photocatalysis. However, to our knowledge, there has been no report on the degradation of the azo dyes by the MPc/TiO_2–H_2O_2 process under visible light. Furthermore, the separation of the nanostructural photocatalysts from the solution after reaction is another challenge in a practical photocatalytic process. The photocatalysts nanoparticles are often limited, because the suspended particulate catalysts are easily lost in the process of photocatalytic reaction and separation, which may repollute the treated water again. The materials with one-dimensional (1D) structural, especially for nanofibers, may overcome the above problems [13,14].

Motivated by the above concerns, we report a successful attempt at the fabrication of 2,9,16,23-tetra-nitrophthalocyanine iron (TNFePc) nanostructure grown on TiO_2 nanofibers substrate by combining the electrospinning technique and the solvothermal method. And the photocatalytic activity of the TNPcFe/TiO_2–H_2O_2 photocatalysts in the visible-light region are investigated by measuring the degradation of methyl orange (MO) as a test substance. In this study, MO has been chosen as a model representative azo dye owing to its wide application in various industries. The experimental results showed that the as-obtained TNFePc/TiO_2–H_2O_2 photocatalysts exhibited excellent visible light photocatalytic activity. Moreover, due to the large length to diameter ratio of TiO_2 nanofibers, the TNFePc/TiO_2 nanofiber heterostructures could be reclaimed easily by sedimentation without a decrease of the photocatalytic activity. Finally, the mechanisms of the visible photocatalysis with the TNFePc/TiO_2 nanofiber heterostructures were proposed.

2. Experimental

2.1. Preparation of TiO_2 nanofibers

First, 2 g of poly(vinylpyrrolidone) powder (PVP, Mw = 13,00,000) was added to a mixture of 9 mL of absolute ethanol and 5 mL of acetic acid in a capped bottle. The obtained solution was stirred for 1 h to generate a homogeneous solution. Then, 2.0 g $Ti(OC_4H_9)_4$ was added to the solution, and the mixture was continuously stirred for another 1 h to make precursor solution. Three milliliters of the precursor solution were placed into a 5 mL syringe, which equipped with a blunt metal needle. The outer diameter and the inner diameter of the needle were 0.8 mm and 0.6 mm, respectively. A stainless steel plate covered with a sheet of aluminum foil was employed as the collector. The distance between the needle tip and collector was 15 cm, and the voltage was set at 9 kV. The as-collected nanofibers were calcined at 550 °C for 2 h to form anatase TiO_2 nanofibers.

2.2. Fabrication of TNFePc/TiO_2 nanofibers

In a typical experiment, 4-nitrophthalonitrile (0.100 mmol), $FeCl_2 \cdot 4H_2O$ (0.025 mmol), ammonium molybdate (1 mg), and TiO_2 nanofibers (15 mg) were put into a 25 mL Teflon-lined stainless autoclave. The autoclave was maintained at 160 °C for 20 h with ethylene glycol up to 80% of the total volume, and then cooled to room temperature naturally. The obtained samples were washed with distilled water under ultrasound, then, dried at 50 °C for 8 h. The as-fabricated sample was denoted as PcT1. When the precursor concentration for synthesizing TNFePc was increased 2 and 4 times, two other samples of TNFePc/TiO_2 were fabricated and were denoted as PcT2 and PcT3, respectively.

2.3. Characterization

The scanning electron microscopy (FESEM, XL-30 ESEM FEG, Micro FEI Philips) and transmission electron microscopy (TEM; high resolution TEM [HRTEM], JEM-3010) were used to characterize the morphologies of the products. Energy dispersive X-ray (EDX) spectroscopy being attached to scanning electron microscopy (SEM) was used to analyze the composition of samples. X-ray diffraction (XRD) measurement was carried out using a D/max 2500 XRD spectrometer (Rigaku) with Cu Kα line of 0.1541 nm. X-ray photoelectron spectroscopy (XPS) was performed on a VG ESCALAB LKII instrument with Mg KR-ADES ($h\nu$ = 1253.6 eV) source at a residual gas pressure of below 10^{-8} Pa. The UV–vis diffuse reflectance (DR) spectroscopy of the sample was recorded on a Cary 500 UV–vis-NIR spectrophotometer. Fourier transform infrared spectra (FT-IR) were obtained on Magna 560 FT-IR spectrometer with a resolution of 1 cm^{-1}.

2.4. Photocatalytic test

The photoreactor was designed with an internal xenon lamp (XHA 150 W and the average intensity was 28 mW/cm^2) equipped with a cut-off glass filter transmitting >400 nm, and the internal light source was surrounded by a water-cooling quartz jacket to cool the lamp. For a typical experiment, a 100 mL of 10 mg L^{-1} methyl orange (MO) solution was mixed with TNFePc/TiO_2 nanocatalyst (0.05 g). The solution was stirred in the dark for 0.5 h to obtain a good dispersion and established adsorption–desorption equilibrium between the organic molecules and the catalyst surface. Then, 2 mL H_2O_2 was added into the mixture. Decreases in the concentrations of dyes were analyzed by a Cary 500 UV–vis-NIR spectrophotometer. At given intervals of illumination, the samples (3 mL) of the reaction solution were taken out and centrifuged. Finally, the filtrates were analyzed.

3. Results and discussion

The morphology of the TiO_2 nanofiber and the TNFePc/TiO_2 nanofiber heterostructures (PcT1) were observed by FE-SEM, which were shown in Fig. 1. Fig. 1a and b shows the typical SEM images of the electrospun TiO_2 nanofibers before solvothermal treatment. From Fig. 1a, it could be observed that the pure TiO_2 aligned in random orientation because of the bending instability associated with the spinning jet. Fig. 1b displayed the corresponding SEM image with higher magnification. It was showed that these randomly oriented TiO_2 had a smooth and uniform surface without secondary nanostructures, and the diameter of the TiO_2 ranged from 250 nm to 300 nm. After solvothermal treatment, the as-fabricated sample remained as a non-woven nanofibers morphology. However, the surface of the TiO_2 nanofiber was no longer smooth. Instead, as shown in Fig. 1c, the nanofibers were decorated with numerous secondary nanosheets. Fig. 1d with high magnification revealed the more detailed structural characteristics of the heterostructures, from which we could see TNFePc nanosheets closely attaching onto the surface of the TiO_2 nanofiber. The TNFePc nanosheets were about 60 nm in thickness and 200–300 nm in size. The EDX spectrum in Fig. 1e demonstrated Ti, O, and C elements existed in pure TiO_2 electropun nanofibers. As expected, the atomic ratio of Ti to O was close to 1:2, whereas, in Fig. 1f, Ti, Fe, O, N, and C was detected in TNFePc/TiO_2 nanofiber heterostructures. Five different places of the TNFePc/TiO_2 nanofiber heterostructures surface were analyzed by EDX, and the mass ratio of TNFePc to TiO_2 was about 9:10, confirming the uniformity of the TNFePc nanosheets grown on the TiO_2 nanofibers.

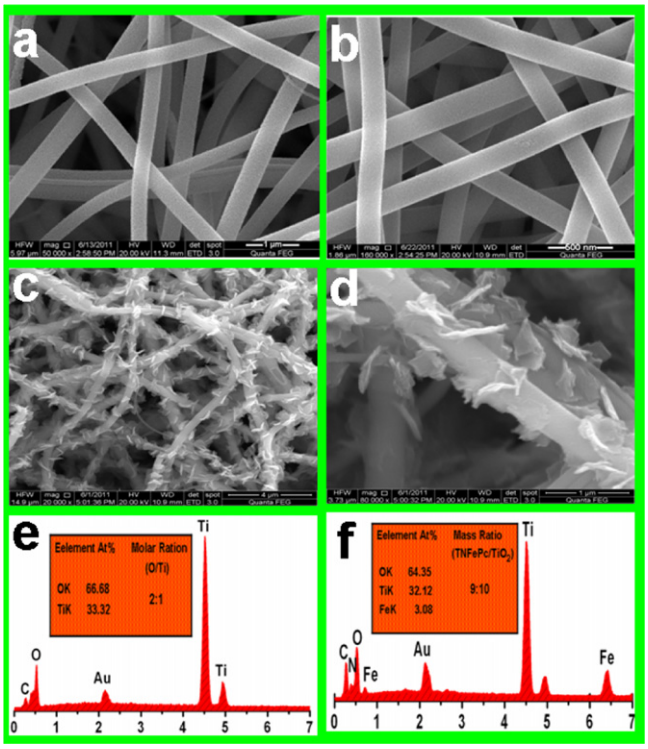

Fig. 1. (a) and (b) SEM images of the TiO_2 nanofiber with different magnifications; (c) and (d) SEM images of the TNFePc/TiO_2 nanofiber heterostructures with different magnifications; (e) and (f) EDX spectra of samples.

In order to obtain the microstructure of the TNFePc/TiO_2 nanofiber heterostructures, the TEM images depicted in Fig. 2 provided a clear observation of the as-synthesized PcT1 sample. The low magnification TEM image of the TNFePc/TiO_2 nanofiber heterostructures was displayed in Fig. 2a. It could be seen that the ultrasonic process during the sample preparation for TEM measurements did not cause the TNFePc nanosheets to fall off the TiO_2, it indicated that TNFePc nanosheets had been successfully grown onto the surface of the TiO_2. Moreover, it could be observed that the diameter of TiO_2 was about 300 nm, which was in agreement with the SEM analysis above. And the TNFePc nanosheets possessed the average size about 200 nm. Meanwhile, a high-resolution image of the TNFePc/TiO_2 nanofiber heterostructures obtained from the area marked with circularity in Fig. 2a were shown in Fig. 2b. The junction displayed two types of clear lattice fringes as shown in Fig. 2b, one set of the fringes spacing was ca. 0.35, corresponding to the

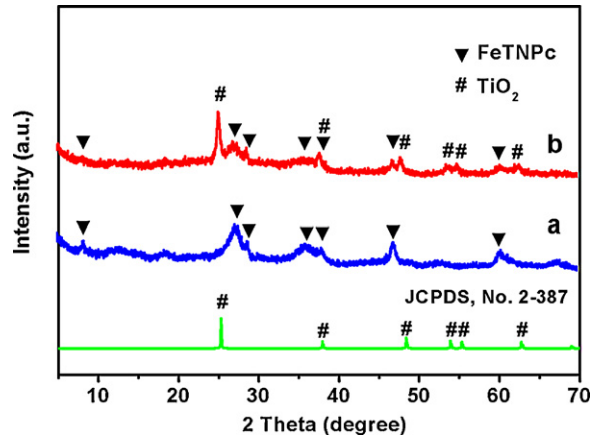

Fig. 3. XRD patterns of the TNFePc (a) and TNFePc/TiO_2 nanofiber heterostructures (b).

(1 0 1) plane of the anatase crystal structure of TiO_2. Another set of disordered stacking feature, corresponding to the low crystallinity of TNFePc. These results confirmed that the heterostructures were well formed between TNFePc nanosheets and TiO_2.

The X-ray diffraction (XRD) patterns of the TNFePc/TiO_2 nanofiber heterostructures and the pure TNFePc were shown in Fig. 3. The curve in Fig. 3a revealed that the crystal phase of the pure TNFePc with the diffraction peaks at about $2\theta = 8.0^\circ$, 26.9°, 28.7°, 36.1°, 38.0°, 46.9° and 60.1°. As for the TNFePc/TiO_2 nanofiber heterostructures in Fig. 3b, except for the diffraction peaks of pure TNFePc, additional diffraction peaks located at 2θ values of 25.5°, 37.9°, 48.2°, 54.1°, and 55.0° could be perfectly indexed to the (1 0 1), (0 0 4), (2 0 0), (1 0 5), and (2 1 1) crystal faces of anatase TiO_2 (PDF card 2-387, JCPDS). No other impurity peaks such as $Fe_4(TiO_4)_3$, or Fe_2O_3 were detected, suggesting that the composition of the above hierarchical nanostructures were TNFePc and TiO_2. Moreover, the average grain sizes of the products was calculated by applying the Debye–Scherrer formula, $D = K\lambda/(\beta \cos\theta)$, where λ was the wavelength of the X-ray radiation (Cu Kα = 0.15406 nm), K was a constant taken as 0.89, β was the line width at half maximum height, and θ was the diffracting angle. The average TNFePc sheet size had been calculated using the three different prominent planes mean value of 208 nm, which was close to the TEM analyses.

The FT-IR spectra of the pure TiO_2 nanofibers, TNFePc/TiO_2 nanofiber heterostructures (PcT1), and TNFePc were shown in Fig. 4. As observed in Fig. 4, the FT-IR spectrum of pure TiO_2 nanofibers only exhibited the absorption peak before 500 cm^{-1},

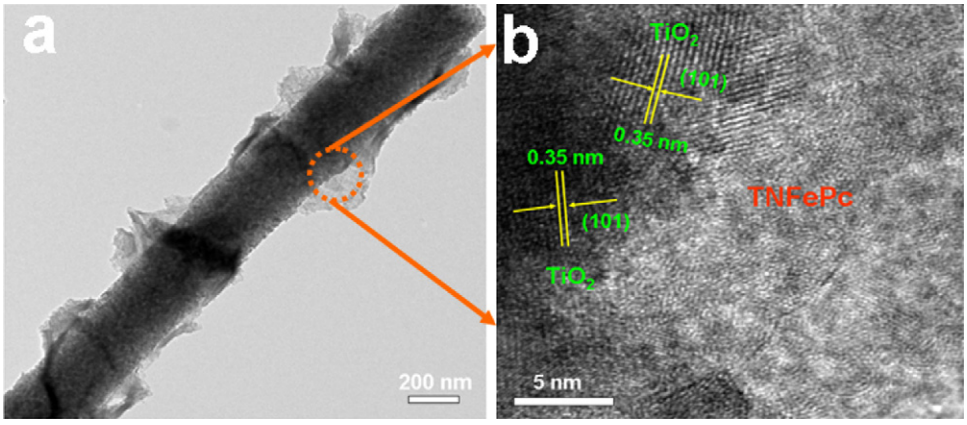

Fig. 2. (a) TEM image of sample PcT1; (b) HRTEM image of the heterojunction region.

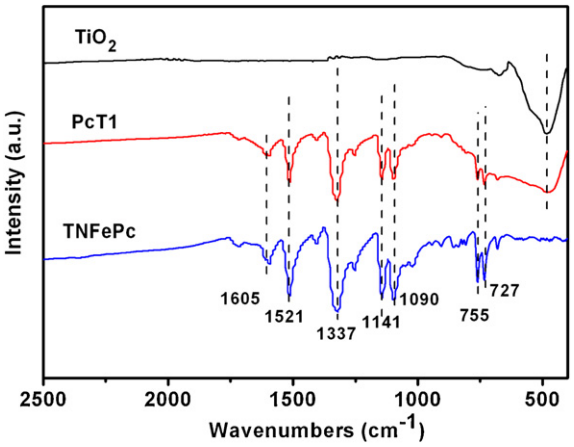

Fig. 4. FT-IR spectra of TiO_2, PcT1 and TNFePc.

which was assigned to the Ti–O vibration. No characteristic peaks for impurity were observed, indicating that all the organic molecules could be removed completely from the PVP/$Ti(OC_4H_9)_4$ composite fibers after calcination at 550 °C, and the pure TiO_2 nanofibers was obtained at this temperature. After solvothermal treatment, the as-fabricated sample PcT1 also appeared several absorption peaks at around 727, 755, 910, 1090, 1141, and 1605 cm^{-1}, which might be assigned to phthalocyanine skeletal and metal–ligand vibrations, respectively [15,16]. The other absorption peaks at 1521, 1337, and 850 cm^{-1} might be assigned to the asymmetric N–O stretching, symmetric N–O stretching and C–NO_2 stretching due to the nitro groups present in the structure of the TNFePc molecule [17]. These peaks were also observed in the FT-IR spectrum of pure TNFePc. The above results revealed that TNFePc was successfully coated onto the surface of TiO_2 nanofibers.

In order to confirm the chemical composition of the prepared nanofiber heterostructures, the sample PcT1 was further studied by XPS analysis and compared with those of the pure TiO_2 nanofiber. Fig. 5a showed the fully scanned spectra. The overview spectra demonstrated that C, Ti, O, Fe and N existed in TNFePc/TiO_2 nanofiber heterostructures, while; C, Ti, and O elements existed in bare TiO_2, respectively. The high-resolution XPS spectra with scanning over the area corresponding to the binding energies for the Ti 2p region around 460 eV were analyzed in Fig. 5b. For the sample PcT1, the peak located at 464.2 eV corresponded to the Ti $2p_{1/2}$ and another one located at 458.5 eV was assigned to Ti $2p_{3/2}$. The splitting between Ti $2p_{1/2}$ and Ti $2p_{3/2}$ was 5.7 eV, indicating a normal state of Ti^{4+} in the TNFePc/TiO_2 nanofiber heterostructures. Besides, the peaks for Ti 2p in the sample PcT1 showed no shift compared with that in pure TiO_2 nanofibers, confirming that the structure of TiO_2 remained intact after synthesis of TNFePc/TiO_2 nanofiber heterostructures. The Fe 2p XPS spectrum could be resolved using the XPS peak fitting program, version 4.1. In Fig. 5c, the most intense pair of doublets for the Fe 2p 3/2 and Fe 2p 1/2 signals at 711 and 725 eV were seen, suggestive of the presence of metallic iron (or its carbide) and oxidized iron species [18]. And, the lower peak at 706.9 eV was attributed to the Fe–N. The N 1s XPS spectrum was shown in Fig. 5d, the lower binding energy component at 398.4 eV was attributed to the pyridyl N, the peak observed at 399.6 eV was pyridyl N associated with metal Fe, affirming peak detected in Fe 2p spectrum due to association with N. The other peaks at 400.4 eV and 405.7 eV were related to pyrrolic N, NO_2^-, respectively [19]. These results further confirmed that the heterostructures were composed of TNFePc and TiO_2. The relative quantitative analysis of each element was completed using the XPS peak area data of different elements and their respective elemental sensitivity factor according to the equation below:

$$\frac{n(E1)}{n(E2)} = \frac{A(E1)/S(E1)}{A(E2)/S(E2)}$$

where n was the number of the atom, E1 and E2 were the element 1 and 2, respectively. A was the peak area, and S was the elemental sensitivity factor [20]. The sensitive factor S of Fe 2p and Ti 2p was 3.69, and 1.80, respectively. Here, the molar ratio of Ti to Fe was about 10:1. The result showed that the value calculated was close to the EDX analyses.

Fig. 6 shows UV–vis diffuse reflectance spectra of the TNFePc, TiO_2 nanofibers and as-prepared TNFePc/TiO_2 nanofiber heterostructures. The spectrum of the TiO_2 nanofibers exhibited the typical absorption behavior of a wide-band-gap oxide semiconductor, having an intense absorption band with a steep edge at about 390 nm. There was no more absorption in visible wavelengths. For the TNFePc/TiO_2 nanofiber heterostructures, the curves of sample PcT1 showed significant red-shift of the absorption edge. It also showed the characteristic absorption of TNFePc around 722 nm, which might be attributable to the Q-band of TNFePc. The Q-band corresponds to excitation between the ground state a1u (π) HOMO to e.g. (π^*) LUMO [21]. This absorption band was also observed in the UV-vis diffuse reflectance spectrum of pure TNFePc. The above results indicated that the sensitization of TiO_2 with TNFePc could extend the absorbance spectrum of TiO_2 into visible region. And, it could possibly lead to a better photocatalytic efficiency, especially under visible-light irradiation.

By simply changing the precursor solution concentration, the secondary TNFePc nanosheets grown on TiO_2 nanofibers with different density could be facilely controlled. From Fig. 7a, it could be seen that the density of the nanosheets grown on the submicron fibers increased significantly when the concentration of the $FeCl_2{\cdot}4H_2O$ precursor was increased 2 times. Moreover, the TNFePc nanosheets were no longer highly dispersed on each fiber. Instead, as shown in Fig. 7b, the nanosheets had been self-assembled into flowerlike architectures. The thickness of the nanosheet increased to about 100 nm and the size had no obvious change. As shown in Fig. 7c, when the concentration of the $FeCl_2{\cdot}4H_2O$ was increased 4 times, there were more flowerlike architectures appeared, which was made up of numerous nanosheets. Fig. 7d was the high magnification of the sample PcT3, from which we could see that almost all of the TiO_2 were covered by TNFePc flowerlike architectures. Fig. 7e showed the EDX spectra of samples PcT2 and PcT3, respectively. The EDX analysis could confirm that the TNFePc loading percentage in TNFePc/TiO_2 nanofiber heterostructures was increased with the increasing of concentration of $FeCl_2{\cdot}4H_2O$. The characteristic peaks of TNFePc and TiO_2 were both observed in the as-obtained samples PcT2 and PcT3, suggesting that the composition of the above nanofibers were TNFePc and TiO_2.

To demonstrate the visible light photoactivity of the as-obtained TNFePc/TiO_2 nanofiber heterostructures for the degradation of organic pollutants, we carried out the experiments of the photocatalytic degradation of methyl orange (MO) as a test reaction, which was a common contaminant in industrial wastewater and had good resistance to light degradation. In the experiments, pure TiO_2 nanofibers used as a photocatalytic reference and the degradation efficiency of the as-prepared samples was defined as C/C_0, where C and C_0 stood for the remnants and initial concentration of MO, respectively. As observed in Fig. 8a, the control experiments were performed under different conditions: (1) in the presence of photocatalysts but in the dark and (2) with visible-light irradiation but in the absence of the photocatalysts. These results illuminated that the adsorption–desorption equilibrium of MO in the dark was established within 30 min. It was seen that the MO solution was very stable and no decomposition in the absence of

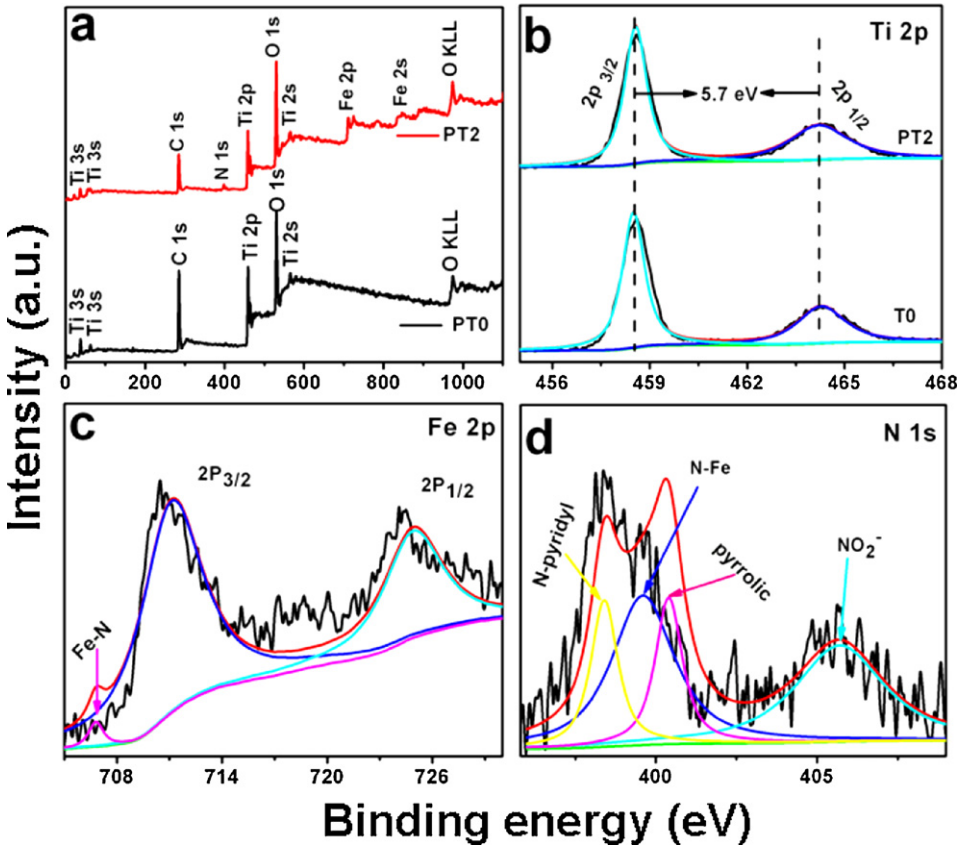

Fig. 5. (a) XPS fully scanned spectra of the samples PcT1 and pure TiO_2 nanofibers; (b) XPS spectra of Ti 2p for the samples PcT1 and pure TiO_2 nanofibers; (c) XPS spectrum of Fe 2p for the sample PcT1; (d) XPS spectra of N 1s for PcT1.

photocatalyst could be observed at all. Fig. 8b showed the degradation curves of MO on the TiO_2 nanofibers, TNFePc/TiO_2 nanofiber heterostructures (PcT1), H_2O_2 assisted TNFePc/TiO_2 nanofiber heterostructures (PcT1, PcT2 and PcT3). As observed in Fig. 8b, because of the large band gap energy (3.2 eV for anatase), TiO_2 nanofibers photocatalysis proceed only at wavelengths shorter than approximately 400 nm. So, TiO_2 nanofibers had a low photocatalytic activity under visible light, and the degradation was only 11% in 3 h. For the TNFePc/TiO_2 nanofiber heterostructures (PcT1), the degradation rate reached 48% in 3 h, which was much higher than that of pure TiO_2 nanofibers. However, it was not effective enough for practical wastewater treatment under visible light irradiation within reasonable time. In contrast, in the presence of H_2O_2, the sample PcT1 exhibited the highest photocatalytic activity. The corresponding degradation rates of MO reached about 94% within 3 h. And the samples PcT2 and PcT3 also displayed good photocatalytic activity under visible light irradiation with the assistance of H_2O_2, the degradation efficiency of MO was about 85, and 69% after 3 h, respectively. Then why did PcT2 and PcT3 show considerably lower activity than PcT1? Although the heterojunction favored electron flow from TNFePc to TiO_2 nanofibers, higher surface coverage of TNFePc nanosheets with aggregation decreased the accessibility of the active sites of the TNFePc nanosheets and TiO_2 nanofibers surface, and thus in turn reduced the photoactivity. All above experimental results suggested that TNFePc as visible-light sensitization improved the visible-light photocatalytic activity of the TNFePc/TiO_2 hierarchical nanostructures. It could be seen that the addition of H_2O_2 could effectively improve the photocatalytic activity, and would greatly promote their industrial application to eliminate the organic pollutants from wastewater.

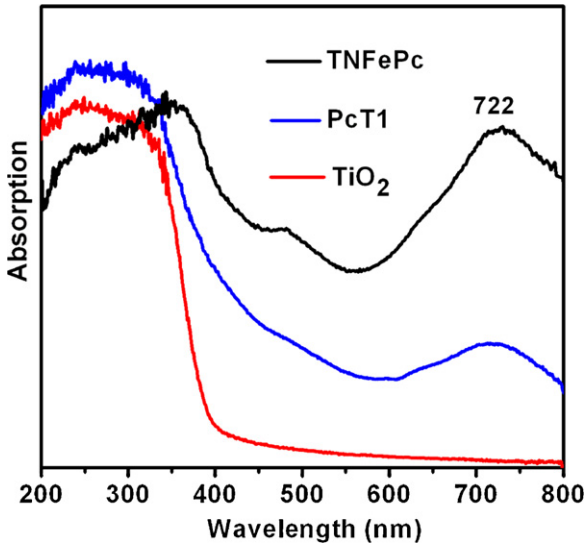

Fig. 6. UV–vis diffuse reflectance spectra of samples TNFePc, PcT1 and TiO_2.

Moreover, the stability of the PcT1 was examined for degradation of dye during a three-cycle experiment, which was very important for the PcT1 to apply in environmental technology. As shown in Table 1, each experiment was carried out under identical conditions, after a three cycle experiment, the degradation efficiency of MO was still over 92%, which revealed the photocatalytic activity of the PcT1 remained almost unchanged.

Based on the above results and the earlier reports on the dye-sensitized photocatalytic oxidation of pollutants, a proposed mechanism of H_2O_2 assisted photocatalytic degradation of MO in visible light irradiation with the TNFePc/TiO_2 nanofiber

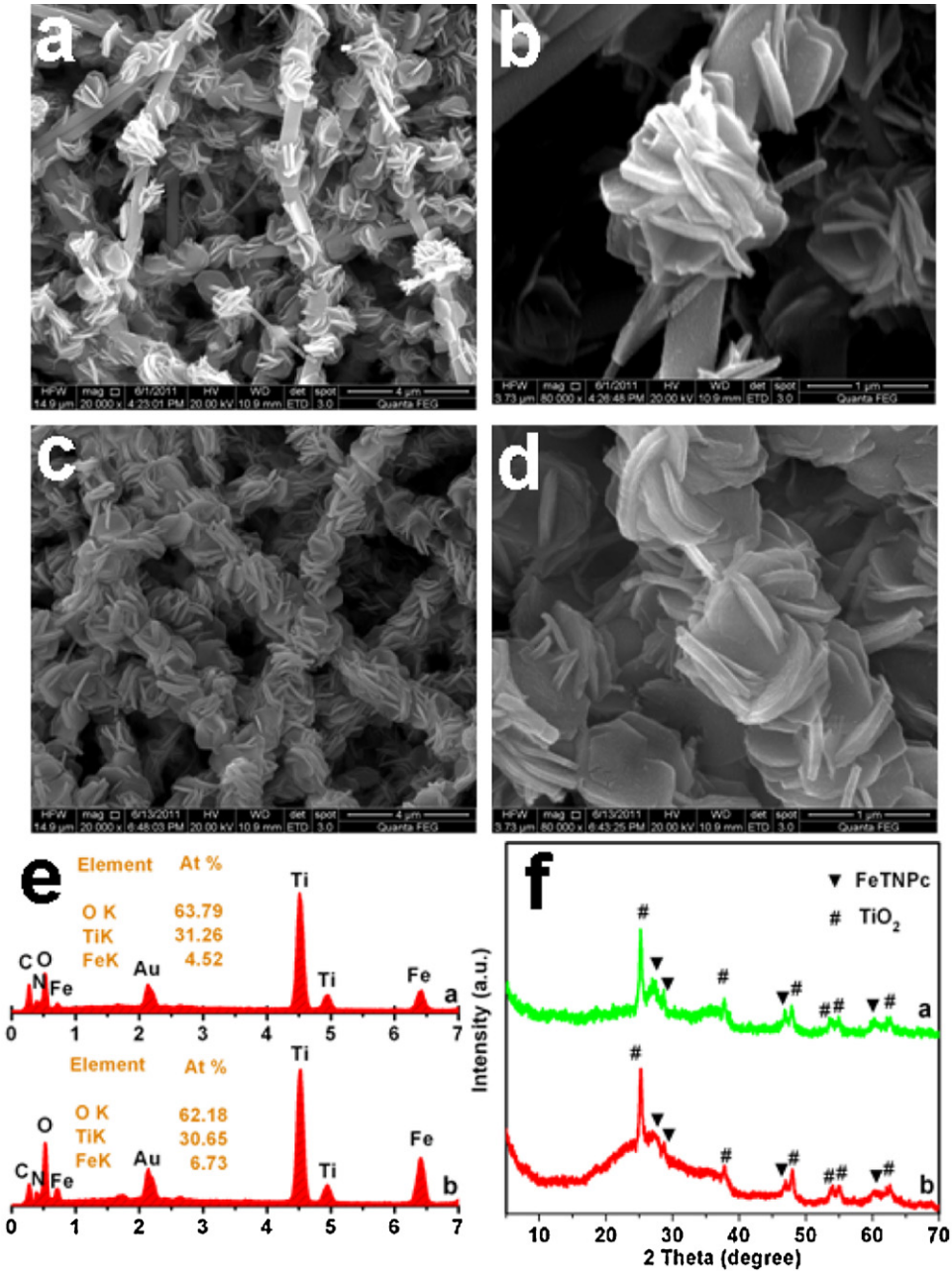

Fig. 7. (a) Low-magnification SEM image of sample PcT2. (b) High-magnification SEM image of the sample PcT2. (c) Low-magnification SEM image of sample PcT3. (d) High-magnification SEM image of the sample PcT3. (e) EDX spectra of samples PcT2 (a) and PcT3 (b). (f) XRD patterns of samples PcT2 (a) and PcT3 (b).

heterostructures was elucidated schematically in Fig. 9. And the mechanism for the photocatalytic degradation of MO in our experiment was proposed as follows:

$$MPc + h\nu \rightarrow MPc^* \quad (1)$$

$$MPc^* + O_2 \rightarrow MPc + {}^1O_2 \quad (2)$$

$$MPc^* + TiO_2 \rightarrow MPc^{\bullet+} + TiO_2(e^-) \quad (3)$$

Table 1
Photocatalytic activity of the sample PcT1 for MO degradation with three times of cycling uses.

Catalyst	Recycling number	Degradation efficiency
PcT1	1st run	93%
	2nd run	92.2%
	3rd run	92%

$$TiO_2(e^-) + (O_2 \text{or} {}^1O_2) \rightarrow TiO_2 + O_2^{\bullet-} \quad (4)$$

$$TiO_2(e^-) + H_2O_2 \rightarrow OH^- + OH^{\bullet} \quad (5)$$

$$O_2^{\bullet-} + H_2O \rightarrow HO_2^{\bullet} + OH^- \quad (6)$$

$$HO_2^{\bullet} + H_2O \rightarrow H_2O_2 + OH^{\bullet} \quad (7)$$

$$H_2O_2 \rightarrow 2OH^{\bullet} \quad (8)$$

$$OH^{\bullet} + MO \rightarrow CO_2 + H_2O \quad (9)$$

$$MPc^{\bullet+} + MO \rightarrow MPc + MO^{\bullet+} \quad (10)$$

The phthalocyanines in the solid state behave as p-type semiconductors, characterized by energy of the band gap about 2.0 eV [22–26]. Upon irradiation with light $\lambda > 400$ nm, it was possible to excite only the phthalocyanine (MPc) particles supported on TiO_2 nanofibers and generated the $^1O_2$ via energy transfer (Eqs. (2) and

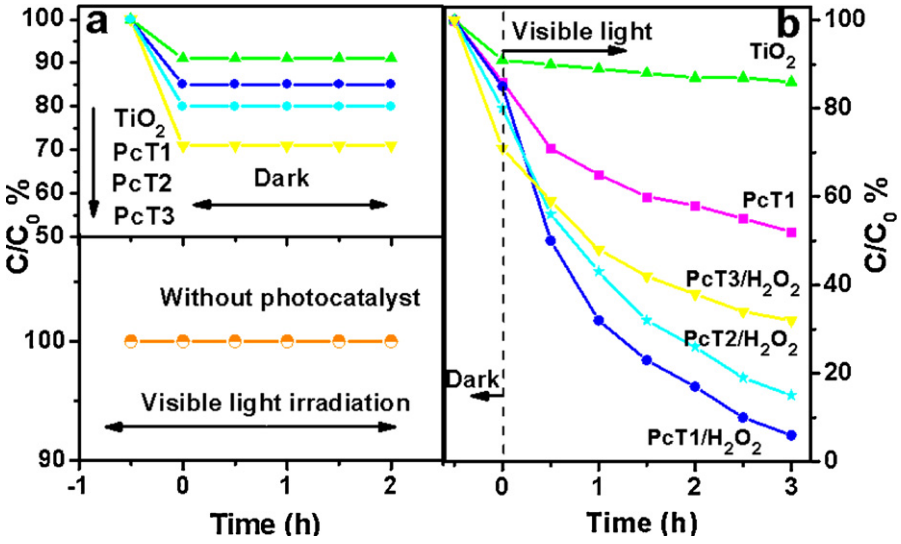

Fig. 8. (a) Degradation profiles of MO in the dark in the presence of the nanofiber photocatalysts and self-degradation of MO with visible light irradiation but in the absence of photocatalysts. (b) Degradation profiles of MO over different samples (C = 10 mg L^{-1}, sample = 0.05 g).

(3)). The excited charge was then injected from the excited state of MPc into the conduction band of TiO_2, followed by generation of the MPc cation radical ($MPc^{\bullet+}$) and conduction band electrons (e_{cb}^-) of TiO_2. Electron injection at the TiO_2 surface was on a subnanosecond time scale, while electron back-transfer from the conduction band to the MPc radical occurred at a rate several orders of magnitude slower than the forward charge injection. Such a rapid electron injection offered more chance for conduction band transport of the injected electrons to surface reaction sites and for the oxidized MPc to react [27]. Dissolved oxygen molecules and singlet oxygen ($^1O_2$) reacted with conduction band electrons (e_{cb}^-) to yield superoxide radical anions ($O_2^{\bullet-}$), which on protonation generated the hydroperoxy radicals ($HO_2^{\bullet}$), producing hydroxyl radicals ($OH^{\bullet}$), which was a powerful oxidizing agent to degrade MO. Because the $TNFePc^{\bullet+}$ radicals had a redox potential of about 1.2 V vs. NHE [28], it could oxidize a suitable substrate, together with recovery of the original TNFePc (Eq. (10)). Inaddition, H_2O_2 had been found to facilitated the generation of hydroxyl radicals and promoted the photodecolorization effectively. And, it could also inhibition of electron/hole (e^-/h^+) pairs recombination according to the following equation [29]:

$$TiO_2(e^-) + H_2O_2 \rightarrow OH^- + OH^{\bullet} \quad (11)$$

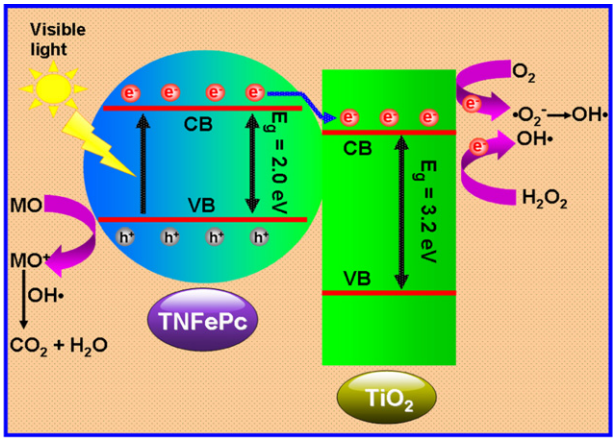

Fig. 9. The proposed mechanisms for the H_2O_2 assistant photocatalysis of the TNFePc/TiO_2 nanofiber heterostructures under visible light irradiation.

4. Conclusion

In summary, the TNFePc/TiO_2 nanofiber heterostructures were successfully fabricated via the electrospinning and solvothermal methods. The as-prepared heterostructures exhibited an excellent photocatalytic efficiency for degradation of MO solution in the presence of H_2O_2 under visible light irradiation ($\lambda > 400$ nm). Furthermore, as their one-dimensional nanostructure property, the TNFePc/TiO_2 nanofiber heterostructures could be easily recycled without decrease of the photocatalytic activity. More importantly, it is expected that the H_2O_2 assistant TNFePc/TiO_2 nanofiber heterostructures with high photocatalytic activity will greatly promote their practical application to eliminate the organic pollutants from wastewater.

Acknowledgements

The present work is supported financially by the National Natural Science Foundation of China (Nos. 50572014, 50972027) and the Program for New Century Excellent Talents in University (NCET-05-0322).

References

[1] L. Kuai, B.Y. Geng, X.T. Chen, Y.Y. Zhao, Y.C. Luo, Facile subsequently light-induced route to highly efficient and stable sunlight-driven Ag–AgBr plasmonic photocatalyst, Langmuir 26 (2010) 18723–18727.
[2] H. Zhang, X.Y. Lv, Y.M. Li, L.M. Li, J.H. Li, P25-Graphene composite as a high performance photocatalyst, ACS Nano 4 (2010) 380–386.
[3] Z. Mesgari, M. Gharagozlou, A. Khosravi, K. Gharanjig, Synthesis, characterization and evaluation of efficiency of new hybrid Pc/Fe–TiO_2 nanocomposite as photocatalyst for decolorization of methyl orange using visible light irradiation, Appl. Catal. A: Gen. 411–412 (2012) 139–145.
[4] S. Kaur, V. Singh, TiO_2 mediated photocatalytic degradation studies of Reactive Red 198 by UV irradiation, J. Hazard. Mater. 141 (2007) 230–236.
[5] W. Baran, A. Makowske, W. Wardas, The effect of UV radiation absorption of cationic and anionic dye solutions on their photocatalytic degradation in the presence TiO_2, Dyes Pigments 76 (2008) 226–230.
[6] J.J. Li, S.Q. Liu, Y.Y. He, J.Q. Wang, Adsorption and degradation of the cationic dyes over Co doped amorphous mesoporous titania–silica catalyst under UV and visible light irradiation, Micropor. Mesopor. Mater. 115 (2008) 416–425.
[7] Z.Y. Zhang, C.L. Shao, L. Zhang, X.H. Li, Y.C. Liu, Electrospun nanofibers of V-doped TiO_2 with high photocatalytic activity, J. Colloid Interface Sci. 351 (2010) 57–62.
[8] J. Zhong, F. Chen, J.L. Zhang, Carbon-deposited TiO_2: synthesis, characterization, and visible photocatalytic performance, J. Phys. Chem. C 114 (2010) 933–939.
[9] Y. Hu, D.Z. Li, Y. Zheng, W. Chen, Y.H. He, Y. Shao, X.Z. Fu, G.C. Xiao, $BiVO_4$/TiO_2 nanocrystalline heterostructure: a wide spectrum responsive photocatalyst

towards the highly efficient decomposition of gaseous benzene, Appl. Catal. B: Environ. 104 (2011) 30–36.
[10] R. Asahi, T. Morikawa, T. Ohwaki, K. Aoki, Y. Taga, Visible-light photocatalysis in nitrogen-doped titanium oxides, Science 293 (2001) 269–271.
[11] M. Zhang, C. Shao, Z. Guo, Z. Zhang, J. Mu, T. Cao, Y. Liu, Hierarchical nanostructures of copper(II) phthalocyanine on electrospun TiO_2 nanofibers: controllable solvothermal-fabrication and enhanced visible photocatalytic properties, ACS Appl. Mater. Interfaces 3 (2011) 369–377.
[12] J. Fernández, J. Kiwi, J. Baeza, J. Freer, C. Lizama, H.D. Mansilla, Orange II photocatalysis on immobilised TiO_2: effect of the pH and H_2O_2, Appl. Catal. B: Environ. 48 (2004) 205–211.
[13] Z.Y. Zhang, C.L. Shao, X.H. Li, L. Zhang, H.M. Xue, Electrospun nanofibers of ZnO–SnO_2 heterojunction with high photocatalytic activity, J. Phys. Chem. C 114 (2010) 7920–7925.
[14] Z.C. Guo, C.L. Shao, J.B. Mu, M.Y. Zhang, Z.Y. Zhang, P. Zhang, B. Chen, Y.C. Liu, Controllable fabrication of cadmium phthalocyanine nanostructures immobilized on electrospun polyacrylonitrile nanofibers with high photocatalytic properties under visible light, Catal. Commun. 12 (2011) 880–885.
[15] R. Seoudi, G.S. El-Bahy, Z.A. El Sayed, FTIR, TGA and DC electrical conductivity studies of phthalocyanine and its complexes, J. Mol. Struct. 753 (2005) 119–126.
[16] T. Kobayashi, R. Kondo, S.J. Nakajima, The metal–ligand vibrations in the infrared spectra of various metal phthalocyanines, Spectrochim. Acta A 26 (1970) 1305–1311.
[17] N.Z. Rajić, D.R. Stojaković, Synthesis and characterization of some nitro-substituted phthalocyanines of nickel(II), cobalt(II) and copper(II), J. Coord. Chem. 19 (1989) 295–301.
[18] S. Maldonado, K.J. Stevenson, Direct preparation of carbon nanofiber electrodes via pyrolysis of iron(II) phthalocyanine: electrocatalytic aspects for oxygen reduction, J. Phys. Chem. B 108 (2004) 11375–11383.
[19] R.L. Arechederra, K. Artyushkova, P. Atanassov, S.D. Minteer, Growth of phthalocyanine doped and undoped nanotubes using mild synthesis conditions for development of novel oxygen reduction catalysts, ACS Appl. Mater. Interfaces 2 (2010) 3295–3302.
[20] J.H. Li, D.Z. Shen, J.Y. Zhang, D.X. Zhao, B.S. Li, Y.M. Lu, Y.C. Liu, X.W. Fan, Magnetism origin of Mn-doped ZnO nanoclusters, J. Magn. Magn. Mater. 302 (2006) 118–121.
[21] L. Edwards, M. Gouterman, X.V. Porphyrins:, Vapor absorption spectra and stability: phthalocyanines, J. Mol. Spectrosc. 33 (1970) 292–310.
[22] D. Schlettwein, M. Kaneko, A. Yamada, D. Woehrle, N.I. Jaeger, Light-induced dioxygen reduction at thin film electrodes of various porphyrins, J. Phys. Chem. 95 (1991) 1748–1755.
[23] R.O. Loutfy, J.H. Sharp, Electronic properties of furanquinone pigments. Correlation between photosensitivity and emissivity, J. Chem. Phys. 71 (1979) 1208–1212.
[24] C.W. Tang, Two-layer organic photovoltaic cell, Appl. Phys. Lett. 48 (1986) 183–185.
[25] Z.D. Popovic, A study of carrier generation in β-metal-free phthalocyanine, Chem. Phys. 86 (1984) 311–321.
[26] V. Iliev, Phthalocyanine-modified titania-catalyst for photooxidation of phenols by irradiation with visible light, J. Photochem. Photobiol. Chem. 151 (2002) 195–199.
[27] N. Bao, Y. Li, Z. Wei, G. Yin, J. Niu, Adsorption of dyes on hierarchical mesoporous TiO_2 fibers and its enhanced photocatalytic properties, J. Phys. Chem. C 115 (2011) 5708–5719.
[28] J.R. Darwent, P. Douglas, A. Harriman, G. Porter, M.C. Richoux, Metal phthalocyanines and porphyrins as photosensitizers for reduction of water to hydrogen, Coord. Chem. Rev. 44 (1982) 83–126.
[29] H.Y. Zhu, R. Jiang, Y.J. Guan, Y.Q. Fu, L. Xiao, G.M. Zeng, Effect of key operational factors on decolorization of methyl orange during H_2O_2 assisted CdS/TiO_2/polymer nanocomposite thin films under simulated solar light irradiation, Sep. Purif. Technol. 74 (2010) 187–194.